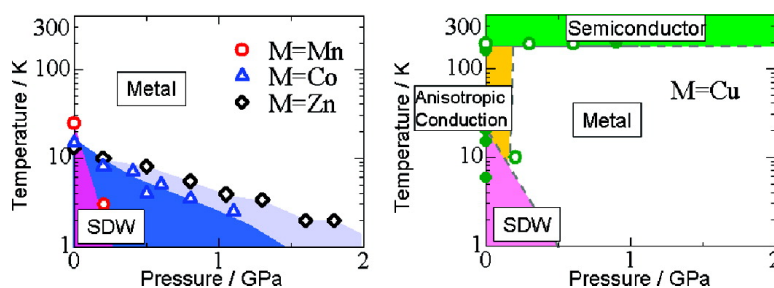


## Metal–Insulator Transition of Charge-Transfer Salts Based on Unsymmetrical Donor DMET and Metal Halide Anions (DMET)(MCI)(TCE) (M = Mn, Co, Cu, Zn; TCE = 1,1,2-trichloroethane)

Hiroshi Ito, Daichi Suzuki, Harutaka Watanabe, Hisaaki Tanaka, Shin-ichi Kuroda, Masamichi Umemiya, Norihito Kobayashi, Makoto Goto, Ken-ichi Sugiura, Hitoshi Miyasaka, Shinya Takaishi, Takashi Kajiwara, Masahiro Yamashita, Eiji Ohmichi, and Toshihito Osada

*J. Am. Chem. Soc.*, **2007**, 129 (27), 8510-8518 • DOI: 10.1021/ja070672q • Publication Date (Web): 16 June 2007

Downloaded from <http://pubs.acs.org> on February 16, 2009



### More About This Article

Additional resources and features associated with this article are available within the HTML version:

- Supporting Information
- Access to high resolution figures
- Links to articles and content related to this article
- Copyright permission to reproduce figures and/or text from this article

[View the Full Text HTML](#)



## Metal–Insulator Transition of Charge-Transfer Salts Based on Unsymmetrical Donor DMET and Metal Halide Anions (DMET)<sub>4</sub>(MCl<sub>4</sub>)(TCE)<sub>2</sub> (M = Mn, Co, Cu, Zn; TCE = 1,1,2-trichloroethane)

Hiroshi Ito,<sup>\*,†</sup> Daichi Suzuki,<sup>†</sup> Harutaka Watanabe,<sup>†</sup> Hisaaki Tanaka,<sup>†</sup> Shin-ichi Kuroda,<sup>†</sup> Masamichi Umemiya,<sup>‡,§</sup> Norihito Kobayashi,<sup>||</sup> Makoto Goto,<sup>||</sup> Ken-ichi Sugiura,<sup>‡</sup> Hitoshi Miyasaka,<sup>‡</sup> Shinya Takaishi,<sup>||</sup> Takashi Kajiwara,<sup>||</sup> Masahiro Yamashita,<sup>||</sup> Eiji Ohmichi,<sup>⊥</sup> and Toshihito Osada<sup>⊥</sup>

Contribution from the Department of Applied Physics, Nagoya University, Chikusa-ku, Nagoya, 464-8603, Japan, Department of Chemistry, Tokyo Metropolitan University, 1-1 Minami-Ohsawa, Hachioji 192-0397, Japan, Department of Chemistry, Tohoku University & CREST, Aramaki, Aoba-ku, Sendai 980-8578, Japan, and Institute of Solid State Physics, University of Tokyo, Kashiwa, 277-8581, Japan

Received January 30, 2007; E-mail: ito@nuap.nagoya-u.ac.jp

**Abstract:** New charge-transfer salts based on an unsymmetrical donor DMET [dimethyl(ethylenedithio)diselenadithiafulvalene] and metal halide anions (DMET)<sub>4</sub>M<sup>II</sup>Cl<sub>4</sub>(TCE)<sub>2</sub> (M = Mn, Co, Cu, Zn; TCE = 1,1,2-trichloroethane) have been synthesized and characterized by transport and magnetic measurements. The crystal structures of the DMET salts are isostructural, consisting of a quasi-one-dimensional stack of DMET and insulating layers containing metal halide anions and TCE. Semimetallic band structures are calculated by the tight-binding approximation. Metal–insulator transitions are observed at  $T_{MI} = 25, 15, 5–20,$  and  $13$  K for M = Mn, Co, Cu, and Zn, respectively. The M = Cu salt exhibits anisotropic conduction at ambient pressure, being semiconducting in the intralayer current direction but metallic for the interplane current direction, down to  $T_{MI}$ . The metal–insulator transitions are suppressed under pressure. In the M = Co and Zn salts, large magnetoresistances with hysteresis are observed at low temperatures, on which Shubnikov–de Haas oscillations are superposed above 30 T. In the M = Cu salt, no hysteresis is observed but clear Shubnikov–de Haas oscillations are observed. The magnetoresistance is small and monotonic in the M = Mn salt. Paramagnetic susceptibilities of the spins of the magnetic ions are observed for the M = Mn, Co, and Cu salts with small negative Weiss temperatures of  $\sim 1$  K. In the nonmagnetic M = Zn salt, Pauli-like  $\pi$ -electron susceptibility that vanishes at  $T_{MI}$  is observed. The ground state of the  $\pi$ -electron system is understood as being a spin density wave state caused by imperfect nesting of the Fermi surfaces. In this  $\pi$ -electron system, the magnetic ions of the M = Mn, Co, and Cu salts interact differently, exhibiting a variety of transport behaviors.

### Introduction

Development of multifunctional molecular materials combining the conducting properties of  $\pi$  electrons with magnetic interactions of transition-metal complexes (d electrons) is a subject of extensive study.<sup>1</sup> When magnetic ions with d electrons are introduced into conducting charge-transfer salts as a counterpart to organic donors having  $\pi$  electrons, an exchange interaction defined as the  $\pi$ –d interaction is present between the donors and anions, which controls electronic conduction and exhibits interesting electronic phenomena. Such a system was first reported for the paramagnetic metal (BEDT-TTF)<sub>3</sub>Cu<sup>II</sup>Cl<sub>4</sub>

H<sub>2</sub>O in which BEDT-TTF molecules form a stable metallic state and Cu<sup>2+</sup>-localized spins show a weak short-range ferromagnetic interaction mediated by the conduction electrons through an RKKY-type interaction.<sup>2</sup> Subsequently, various fascinating electronic phenomena associated with  $\pi$ –d interactions have been observed, such as paramagnetic superconductivity in (BEDT-TTF)<sub>4</sub>(H<sub>3</sub>O)Fe<sup>III</sup>(C<sub>2</sub>O<sub>4</sub>)<sub>3</sub>(C<sub>6</sub>H<sub>5</sub>CN),<sup>3</sup> antiferromagnetic superconductivity in  $\kappa$ -(BETS)<sub>2</sub>Fe<sup>III</sup>Br<sub>4</sub><sup>4</sup> (BETS = bis(ethylenedithio)tetraselenafulvalene), the ferromagnetic metallic state in (BEDT-TTF)<sub>3</sub>[Mn<sup>II</sup>Cr<sup>III</sup>(C<sub>2</sub>O<sub>4</sub>)<sub>3</sub>],<sup>5</sup> and field-induced superconductivity in  $\lambda$ -(BETS)<sub>2</sub>Fe<sup>III</sup>Cl<sub>4</sub>.<sup>6</sup>

<sup>†</sup> Nagoya University.

<sup>‡</sup> Tokyo Metropolitan University.

<sup>§</sup> Present address, Department of Material Science, University of Hyogo, Kamigori, Hyogo 678-1297, Japan.

<sup>||</sup> Tohoku University & CREST.

<sup>⊥</sup> University of Tokyo.

(1) Enoki, T.; Miyazaki, A. *Chem. Rev.* **2004**, *104*, 5449–5477.

(2) Day, P.; Kurmoo, M.; Mallah, T.; Marsden, I. R.; Friend, R. H.; Pratt, F. L.; Hayes, W.; Chasseau, D.; Caultier, J.; Bravic, G.; Ducasse, L. *J. Am. Chem. Soc.* **1992**, *114*, 10722–10729.

(3) Kurmoo, M.; Graham, A. W.; Day, P.; Coles, S. J.; Hursthouse, M. B.; Caulfield, J. M.; Singleton, J.; Ducasse, L.; Guionneau, P. *J. Am. Chem. Soc.* **1995**, *117*, 12209–12217.

(4) Ojima, E.; Fujiwara, H.; Kato, K.; Kobayashi, H.; Tanaka, H.; Kobayashi, A.; Tokumoto, M.; Cassoux, P. *J. Am. Chem. Soc.* **1999**, *121*, 5581–5582.

The unsymmetrical donor dimethyl(ethylenedithio)diselenadithiafulvalene (DMET) has produced many organic conductors and superconductors,<sup>7–8</sup> the most recently discovered being (DMET)<sub>2</sub>Cu<sup>I</sup>Cl<sub>2</sub>.<sup>9</sup> The DMET molecule consists of one-half a TMTSF molecule and one-half a BEDT-TTF molecule. On the basis of its hybrid nature, DMET salts exhibit a variety of structures from quasi-one-dimensional (Q1D) structures to a two-dimensional  $\kappa$ -type structure sandwiched by anion insulating layers. For the Q1D structure with an intercolumnar interaction between the DMET stacks, the Q1D electronic band structure can be calculated by tight-binding band approximations of the highest-occupied molecular orbitals (HOMOs) of the DMET molecules. The Q1D electronic band structure is well characterized quantitatively by angle-dependent magnetoresistance, thermopower, and polarized reflectance measurements.<sup>9,10</sup> On the basis of the Q1D band structure, DMET salts exhibit interesting electronic phenomena such as unconventional superconductivity and field-induced spin density wave (FISDW) transitions.<sup>11</sup> DMET salts present an alternative example of Q1D metals to the well-studied TMTSF salts.

The  $\pi$ -d interactions in (DMET)<sub>2</sub>Fe<sup>III</sup>Br<sub>4</sub> molecules have been studied in detail.<sup>12</sup> These compounds have crossed double-column structures with DMET molecules sandwiched between metal halide layers. The  $\pi$ -electron system shows a metal-insulator (MI) transition at 40 K and a spin density wave (SDW) transition below 25 K. Below 3.7 K, antiferromagnetic ordering of Fe spins is observed. The low-temperature  $\pi$ -electron state under antiferromagnetic ordering has been studied by measurements of magnetization and magnetoresistance in terms of weak ferromagnetic phase transitions due to  $\pi$ -d interactions. We recently reported a new example of a  $\pi$ -d system of a DMET with a Cr complex (DMET)<sub>3</sub>[Cr<sup>III</sup>(isoq)<sub>2</sub>(NCS)<sub>4</sub>] and (DMET)<sub>3</sub>[Cr<sup>III</sup>(phen)(NCS)<sub>4</sub>]CH<sub>3</sub>CN having negative Weiss temperature.<sup>13</sup>

In this paper we report on the synthesis and electronic characteristics of the new charge-transfer salts consisting of DMET molecules with metal halide anions (DMET)<sub>4</sub>M<sup>II</sup>Cl<sub>4</sub>(TCE)<sub>2</sub> (M = Mn, Co, Cu, Zn; TCE = 1,1,2-trichloroethane), studied by transport and magnetic measurements. The four salts are isostructural with Q1D stacks of DMET molecules sandwiched between anion and TCE layers. Unlike other Q1D

systems, the DMET molecules in the salts are weakly tetramerized. The Q1D Fermi surfaces are folded, resulting in semimetallic Fermi surfaces consisting of electron and hole pockets, similar to the anion-ordered state of (TMTSF)<sub>2</sub>NO<sub>3</sub>.<sup>14</sup> The present isostructural series of salts with magnetic (Mn, Co, Cu) and nonmagnetic (Zn) ions provides a novel model to investigate  $\pi$ -d interactions in charge-transfer salts.

## Experimental Section

**Syntheses.** DMET was synthesized by the reported method and recrystallized from CS<sub>2</sub>/hex.<sup>15</sup> (<sup>n</sup>Bu<sub>4</sub>N)<sub>2</sub>(M<sup>II</sup>Cl<sub>4</sub>) (M = Mn, Co, Cu, Zn) was prepared by metathesis of (<sup>n</sup>Bu<sub>4</sub>N)Cl and metal halides in ethanol and recrystallized from small amounts of 1,2-dichloroethane.<sup>16</sup> Single crystals were prepared by the electrochemical oxidation of DMET (6 mg, 1.4 × 10<sup>-5</sup> mol) in 1,1,2-trichloroethane (20 mL) with the corresponding tetrabutylammonium salts (<sup>n</sup>Bu<sub>4</sub>N)<sub>2</sub>(M<sup>II</sup>Cl<sub>4</sub>) (25–30 mg, 3.6 × 10<sup>-5</sup> mol) as a supporting electrolyte under nitrogen atmosphere at 15 °C. The 1,1,2-trichloroethane was distilled from CaH<sub>2</sub> before use. A two-compartment glass H cell equipped with platinum electrodes was used. The current was kept constant at 0.2–0.5  $\mu$ A for 2 weeks. The typical size of the obtained block-shaped crystals was 0.4 × 0.3 × 0.1 mm<sup>3</sup> for all salts. The long axis of the crystal corresponded to either the *a* + *b* or *a* direction.

**X-ray Crystallography.** Single crystals were mounted on a glass rod with silicon grease. X-ray diffraction data for M = Mn, Co, and Cu salts were collected at 113 K using a Rigaku AFC7R diffractometer with graphite-monochromated Mo K $\alpha$  radiation and a rotating anode generator ( $\lambda = 0.71069$  Å, 50 kV, 100 mA,  $2\theta \leq 55^\circ$ ,  $\omega - 2\theta$  technique). X-ray diffraction data for the M = Zn salt were collected at 113 K using a Rigaku Saturn CCD area detector with graphite-monochromated Mo K $\alpha$  radiation ( $\lambda = 0.71070$  Å, 50 kV, 40 mA,  $2\theta \leq 62^\circ$ ). The data were corrected for Lorentz and polarization effects. The structures were solved by direct methods (SIR 97) and refined on the structural factor  $F^2$  by a full-matrix least-squares methods using SHELX programs.<sup>17</sup> The non-hydrogen atoms were refined anisotropically, while the hydrogen atoms were introduced as fixed contributors. All calculations were performed using the CrystalStructure crystallographic software package.<sup>18</sup> Summaries of the crystallographic data collection and refinement parameters are given in Table 1.

**Band Calculation.** The overlap integrals ( $S$ ) between the HOMOs of the DMET molecules were calculated by the extended Hückel method using the semiempirical Hückel parameters.<sup>19</sup> The band structures were calculated by the tight-binding band approximation with transfer integrals evaluated by  $t = ES$ , where  $E$  is the energy of the HOMO,  $E = -10$  eV.

**Electrical Properties.** The electrical resistivity was measured using the four-terminal dc method with a measuring current of 1–0.01  $\mu$ A. Four platinum wires were attached to a single crystal with carbon paste for in-plane (*ab* plane) and interplane (*c* axis) resistivity measurements. The measuring current was alternated in order to eliminate thermoelectric effects. The electrical resistivity under pressure was measured

- (5) Coronado, E.; Galan-Mascaros, J. R.; Gomez-Garcia, C. J.; Laukhin, V. *Nature* **2000**, *408*, 447–.
- (6) Uji, S.; Shinagawa, H.; Terashima, T.; Yakabe, T.; Terai, Y.; Tokumoto, M.; Kobayashi, A.; Tanaka, H.; Kobayash, H. *Nature* **2001**, *410*, 908–910.
- (7) Ishiguro, T.; Yamaji, K.; Saito, G. *Organic Superconductors*, 2nd ed.; Springer-Verlag: Berlin, 1998.
- (8) Murata, K.; Kikuchi, K.; Takahashi, T.; Honda, Y.; Saito, K.; Kanoda, K.; Tokiwa, T.; Anzai, H.; Ishiguro, T.; Ikemoto, I. *J. Mol. Elec.* **1988**, *4*, 173–179.
- (9) Ito, H.; Suzuki, D.; Yokochi, Y.; Kuroda, S.; Umemiya, M.; Miyasaka, H.; Sugiura, K.-I.; Yamashita, M.; Tajima, H. *Phys. Rev. B* **2005**, *71*, 212503–1–4.
- (10) (a) Kikuchi, K.; Neriishi, K.; Miyazaki, K.; Saito, K.; Ikemoto, I.; Kobayashi, K. *Synth. Met.* **1993**, *41–43*, 2275–2280. (b) Yoshino, H.; Murata, K.; Saito, K.; Nishikawa, H.; Kikuchi, K.; Ikemoto, I. *Phys. Rev. B* **2003**, *67*, 035111–1–9.
- (11) (a) Uji, S.; Terakura, C.; Terashima, T.; Aoki, H.; Nishikawa, H.; Ikemoto, I.; Kikuchi, K. *Proceedings of the Physical Phenomena at High Magnetic Fields III*; World Scientific: London, 1998; pp 277–280. (b) Ito, H.; Yokochi, Y.; Suzuki, D.; Tanaka, H.; Kuroda, S.; Enomoto, K.; Uji, S.; Umemiya, M.; Miyasaka, H.; Sugiura, K.-I.; Yamashita M. *Synth. Met.* **2006**, *156*, 162–165.
- (12) Enomoto, K.; Yamaura, J.; Miyazaki, A.; Enoki, T. *Bull. Chem. Soc. Jpn.* **2003**, *76*, 945–959.
- (13) Umemiya, M.; Goto, M.; Kobayashi, N.; Takaishi, S.; Kajiwara, T.; Yamashita, M.; Miyasaka, H.; Sugiura, K.; Watanabe, H.; Suzuki, D.; Ito, H.; Kuroda, S. *Chem. Lett.* **2006**, *35*, 368–369.

- (14) (a) Grant, P. M. *Phys. Rev. Lett.* **1983**, *50*, 1005–1008. (b) Osada, T.; Shinagawa, H.; Kagoshima, S.; Miura, N. *Synth. Met.* **1993**, *55–57*, 1795–1802.
- (15) (a) Kikuchi, K.; Namiki, T.; Ikemoto, I.; Kobayashi, K. *J. Chem. Soc., Chem. Commun.* **1986**, 1472–1473. (b) Svenstrup, N.; Becher, J. *Synthesis* **1995**, 215–235. (c) Moradpour, A.; Peyrussan, V.; Johansen, I.; Bechgaard, K. *J. Org. Chem.* **1983**, *48*, 388–389.
- (16) Cotton, F. A.; Goodgame, D. M. L.; Goodgame, M. *J. Am. Chem. Soc.* **1962**, *84*, 167–168.
- (17) Sheldrick, G. M. *SHELX97: Programs for Crystal Structure Analysis (Release 97-2)*; Institut für Anorganische Chemie der Universität: Göttingen, Germany, 1998.
- (18) *CrystalStructure 3.6.0: Crystal Structure Analysis Package*; Rigaku and Rigaku/MS: The Woodlands, TX, 2000–2004.
- (19) Mori, T.; Kobayashi, A.; Sasaki, Y.; Kobayashi, H.; Saito, G.; Inokuchi, H. *Bull. Chem. Soc. Jpn.* **1984**, *57*, 627. The parameters of Slater atomic orbitals [ $\zeta$  exponent, ionization potential (eV)] are as follows: Se, 4s (2.112, -1.471), 4p (1.827, -0.809); S, 3s (2.112, -1.62), 3p (1.827, -0.77); C, 2s (1.625, -1.573), 2p (1.625, -0.838); H, 1s (1.0, -1.0).

**Table 1.** Crystallographic Data and Refinement Parameters for the Four Salts

	M = Mn	M = Co	M = Cu	M = Zn
formula	C <sub>44</sub> H <sub>46</sub> Cl <sub>10</sub> -MnS <sub>16</sub> Se <sub>8</sub>	C <sub>44</sub> H <sub>46</sub> Cl <sub>10</sub> -CoS <sub>16</sub> Se <sub>8</sub>	C <sub>44</sub> H <sub>46</sub> Cl <sub>10</sub> -CuS <sub>16</sub> Se <sub>8</sub>	C <sub>44</sub> H <sub>46</sub> Cl <sub>10</sub> -S <sub>16</sub> Se <sub>8</sub> Zn
fw	2128.96	2132.95	2137.56	2139.40
shape	block	block	block	block
cryst syst	triclinic	triclinic	triclinic	triclinic
space group	P1 (no. 1)	P1 (no. 1)	P1 (no. 1)	P1 (no. 1)
a/Å	8.884(8)	8.866(2)	8.919(5)	8.8579(10)
b/Å	10.569(2)	10.561(2)	10.512(2)	10.5377(11)
c/Å	18.114(2)	18.086(4)	17.912(2)	18.060(2)
α/deg	82.10(2)	82.19(2)	83.21(2)	82.204(3)
β/deg	88.22(2)	88.02(2)	88.43(2)	88.008(3)
γ/deg	84.79(1)	84.76(1)	84.81(1)	84.742(3)
V/Å <sup>3</sup>	1677(1)	1670.4(6)	1660.4(9)	1662.7(3)
Z	1	1	1	1
D <sub>calcd</sub> /g cm <sup>-3</sup>	2.107	2.120	2.138	2.136
T/K	113 ± 1	113 ± 1	113 ± 1	113 ± 1
F <sub>000</sub>	1033.00	1035.00	1037.00	1038.00
no. of reflns measured (total)	9384	9338	9279	11871
observed	9384 (all reflns)	9338 (all reflns)	9279 (all reflns)	11871 (all reflns)
GOF	1.024	1.016	1.016	1.043
R1 <sup>a</sup>	0.030 ( <i>I</i> > 2.00σ( <i>I</i> ))	0.030 ( <i>I</i> > 2.00σ( <i>I</i> ))	0.029 ( <i>I</i> > 2.00σ( <i>I</i> ))	0.037 ( <i>I</i> > 2.00σ( <i>I</i> ))
wR2 <sup>b</sup>	0.082 (all reflns)	0.083 (all reflns)	0.080 (all reflns)	0.106 (all reflns)

$$^a R1 = \sum ||F_o| - |F_c|| / \sum |F_o|. \quad ^b wR2 = [\sum (w(F_o^2 - F_c^2)^2) / \sum w(F_o^2)^2]^{1/2}.$$

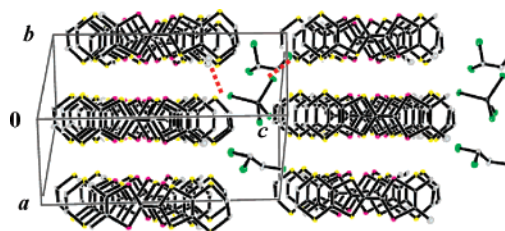
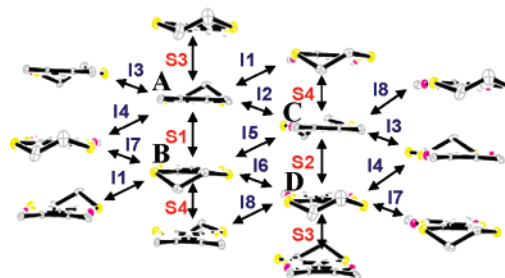
with a Be–Cu clamp-type cell. Pressure was applied via Daphne 7373 oil at room temperature, and the cell was clamped with screws. The pressure decreased by ~0.2 GPa at low temperatures compared to room temperature.<sup>20</sup> The temperature was monitored with a calibrated Cernox thermometer. The magnetoresistance was measured up to 40 T using a long-duration (60 ms) pulsed magnet with a <sup>3</sup>He cryostat. Transient voltage curves under a constant current of 10–50 μA were recorded with a Nicolet Pro 40 digitizer with a preamplifier.

**Magnetic Susceptibility.** The magnetic susceptibilities of the polycrystalline samples were measured with a SQUID magnetometer (Quantum Design MPMS-7) in the temperature range 1.8–300 K. Diamagnetic correction was carried out by subtracting Pascal's constants.<sup>21</sup>

**Electron Spin Resonance.** Electron spin resonance (ESR) spectra were measured with an X-band ESR spectrometer (Bruker EMX) equipped with a gas-flow cryostat (Oxford 900). A single crystal was mounted on a mylar (polyethylene–terephthalate) film with a small amount of grease so that the *ab* plane was perpendicular to the external field of the ESR spectrometer and inserted into a quartz sample tube of 3 mm inner diameter. The absolute magnitude of the susceptibility and *g* value were calibrated using CuSO<sub>4</sub>·5H<sub>2</sub>O and diphenylpicrylhydrazyl (DPPH) as standards, respectively.

## Results

**Crystal Structures.** X-ray structural analysis revealed that all the DMET salts are isostructural with each other. The crystal structure for M = Mn is shown in Figure 1. The unit cell contains four crystallographically independent DMET molecules, one MnCl<sub>4</sub><sup>2-</sup> anion, and two TCE solvent molecules. The DMET molecules are alternately stacked in a face-to-face manner to form Q1D columns along the *a* + *b* axis. The arrangement of the DMET molecules within the *ab* plane is shown in Figure 2. The interplanar distances of the DMET molecules, calculated from the mean plane, range from 3.51 to

**Figure 1.** Crystal structure of (DMET)<sub>4</sub>MnCl<sub>4</sub>(TCE)<sub>2</sub>. The dotted lines represent short S···Cl contacts less than the sum of the van der Waals radii.**Figure 2.** Molecular arrangement within the conducting *ab* plane of (DMET)<sub>4</sub>MnCl<sub>4</sub>(TCE)<sub>2</sub>. The bond lengths for the four independent DMET molecules (A–D) are listed in Table 2. The arrows indicate the overlap integrals between the HOMOs of the DMET molecules listed in Table 3.

3.53 Å. The short intercolumnar S···S and Se···Se distances between the DMET molecules (e.g., S···S = 3.42–3.54 Å, Se···Se = 3.77–3.79 Å) were observed to be less than the sum of the van der Waals radii. Other meaningful contacts along DMET columns may be considered as hydrogen bonds (e.g., S···H ≈ 2.93 Å). The presence of intermolecular contacts suggests that the system behaves as a Q1D electronic system.

The measured bond lengths for the four independent DMET molecules (A–D) are listed in Table 2 for all four salts. The empirical correlation of the bond lengths in the donor molecules is a useful tool for evaluating the degree of charge transfer. It is known that the C=C bond length increases and C–Se and C–S bond lengths decreases as the oxidation of the donor increases. The C=C bond lengths of the four independent DMET molecules are almost the same for each salt, which suggests that the four DMET molecules have the same charge of +0.5. The DMET molecules for the M = Mn, Co, and Zn salts have central C=C bond lengths ranging from 1.36 to 1.37 Å, which is consistent with that of (DMET)<sub>2</sub>CuCl<sub>2</sub> with a DMET charge of +0.5. For the M = Cu salt, the C=C bond lengths range from 1.37 to 1.38 Å and may be slightly longer compared to the other salts. Hence, there may be a slight positive deviation of the averaged valence state from +0.5 in the M = Cu salt, in which case some of the Cu ion must turn monovalent to maintain neutrality.

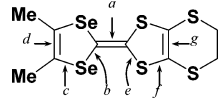
The insulating layers of the M = Mn salts contain MnCl<sub>4</sub><sup>2-</sup> anions and TCE solvent molecules. In the insulating layers, several intermolecular short contacts with CH···Cl hydrogen bonds have been determined [e.g., Cl···Cl (MnCl<sub>4</sub><sup>2-</sup>–TCE) contacts = 3.487 Å, Cl···Cl (TCE–TCE) contacts = 3.372, 3.465 Å, CH···Cl hydrogen (TCE–MnCl<sub>4</sub><sup>2-</sup>) bonds = 2.681, 2.864 Å]. The TCE solvent molecules are strongly incorporated in the cavity between the MnCl<sub>4</sub><sup>2-</sup> ions and do not evaporate. These compounds are stable as single crystals for more than 1 year.

The MnCl<sub>4</sub><sup>2-</sup> moieties have tetrahedral coordination geometry. The Mn–Cl bond lengths are 2.365(2) Å on average, and

(20) Murata, K.; Yoshino, H.; Yadav, H. O.; Honda, Y.; Shirakawa, N. *Rev. Sci. Instrum.* **1997**, *68*, 2490–2493.

(21) Kahn O. *Molecular Magnetism*; VCH Publishers: New York, 1993.



**Table 2.** Bond Lengths of the Four DMET Molecules (A–D) in the Unit Cell for the Four Salts


	$\rho$	a	b	c	d	e	f	g	
DMET	0	1.334(6)	1.904(4)	1.906(4)	1.341(6)	1.764(4)	1.758(5)	1.383(6)	
(DMET) <sub>2</sub> CuCl <sub>2</sub>	+0.5	1.356(5)	1.879(3)	1.903(3)	1.342(4)	1.753(3)	1.755(3)	1.359(4)	
(DMET) <sub>4</sub> (MnCl <sub>4</sub> )(TCE) <sub>2</sub>	A	+0.5	1.37(1)	1.879(7)	1.894(7)	1.36(1)	1.732(7)	1.763(7)	1.334(9)
	B	+0.5	1.36(1)	1.876(7)	1.898(7)	1.331(9)	1.745(7)	1.741(7)	1.37(1)
	C	+0.5	1.36(1)	1.880(7)	1.898(7)	1.350(9)	1.744(7)	1.763(7)	1.351(9)
	D	+0.5	1.37(1)	1.876(7)	1.904(7)	1.337(9)	1.745(7)	1.742(7)	1.355(9)
(DMET) <sub>4</sub> (CoCl <sub>4</sub> )(TCE) <sub>2</sub>	A	+0.5	1.36(1)	1.875(8)	1.890(8)	1.36(1)	1.755(8)	1.751(8)	1.35(1)
	B	+0.5	1.37(1)	1.879(8)	1.900(8)	1.35(1)	1.734(8)	1.749(8)	1.36(1)
	C	+0.5	1.37(1)	1.878(8)	1.894(8)	1.35(1)	1.741(8)	1.757(8)	1.36(1)
	D	+0.5	1.36(1)	1.880(8)	1.906(8)	1.33(1)	1.739(8)	1.752(8)	1.35(1)
(DMET) <sub>4</sub> (CuCl <sub>4</sub> )(TCE) <sub>2</sub>	A	+0.5	1.368(9)	1.884(7)	1.893(7)	1.357(9)	1.736(7)	1.756(7)	1.351(9)
	B	+0.5	1.378(9)	1.870(7)	1.916(7)	1.320(9)	1.747(7)	1.747(7)	1.358(9)
	C	+0.5	1.372(9)	1.881(6)	1.900(7)	1.347(9)	1.740(7)	1.762(7)	1.339(9)
	D	+0.5	1.38(1)	1.872(7)	1.907(7)	1.320(9)	1.736(7)	1.752(7)	1.363(9)
(DMET) <sub>4</sub> (ZnCl <sub>4</sub> )(TCE) <sub>2</sub>	A	+0.5	1.369(9)	1.866(6)	1.899(6)	1.358(8)	1.746(6)	1.755(7)	1.338(8)
	B	+0.5	1.365(9)	1.885(6)	1.898(6)	1.334(8)	1.737(7)	1.751(7)	1.366(9)
	C	+0.5	1.362(9)	1.869(6)	1.906(6)	1.352(8)	1.748(6)	1.750(7)	1.351(8)
	D	+0.5	1.367(9)	1.878(6)	1.893(6)	1.329(8)	1.742(6)	1.759(7)	1.350(8)
(DMET)(I <sub>3</sub> ) <sub>2</sub>	+2.0	1.41(1)	1.847(5)	1.887(7)	1.33(2)	1.725(5)	1.741(7)	1.35(2)	

the Cl–Mn–Cl bond angles are in the range 104.38(8)–114.68(8)°. These values are similar to those previously reported for Mn<sup>II</sup>Cl<sub>4</sub><sup>2-</sup> species, e.g., 2.361(2) Å and 108.55(8)–111.14(9)° for (Me<sub>4</sub>N)<sub>2</sub>(MnCl<sub>4</sub>).<sup>22</sup> The environments of the metal center for the M = Co, Cu, and Zn salts are also common for divalent halides. The observed average M–Cl bond lengths and Cl–M–Cl bond angles are 2.288(2) Å and 104.86(8)–114.19(8)° for CoCl<sub>4</sub>, 2.256(2) Å and 99.94(7)–126.91(8)° for CuCl<sub>4</sub>, and 2.270(2) Å and 105.39(7)–114.37(8)° for ZnCl<sub>4</sub>. These bond lengths and angles are in good agreement with previous reports on corresponding divalent anions.<sup>23–25</sup> From the results for the C=C and M<sup>II</sup>–Cl bond lengths the charge on each DMET molecule is considered to be +0.5. For the CuCl<sub>4</sub><sup>2-</sup> anion we found no evidence for the presence of monovalent species. The larger deviation of the bond angles of the CuCl<sub>4</sub><sup>2-</sup> anion from tetrahedral symmetry is caused by Jahn–Teller distortion of the Cu<sup>II</sup> ion.<sup>2</sup>

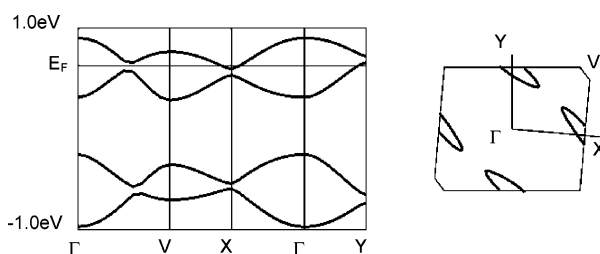
The nearest neighboring distance between two metal atoms is about 9 Å, corresponding to the length of the *a* axis. Short S···Cl contacts between the DMET molecules and MCl<sub>4</sub><sup>2-</sup> were observed [3.296(3) and 3.507(3) Å for Mn, 3.315(3) and 3.506(3) Å for Co, 3.456(3) and 3.548(3) Å for Cu, 3.313(3) and 3.499(2) Å for Zn] and associated with a magnetic interaction between the  $\pi$  electron of the DMET molecules and the *d* electron of the MCl<sub>4</sub> anions.

**Electronic Structures.** The calculated overlap integrals of the HOMOs of the DMET molecules are listed in Table 3 with the arrangement of the DMET molecules within the *ab* plane shown in Figure 2. The *d* orbitals of the S and Se atoms were not included in the calculations. The overlap integrals along

**Table 3.** Calculated Overlap Integrals (*S*) ( $\times 10^{-3}$ ) of the HOMOs of the DMET Molecules for the Four Salts

	M = Mn	M = Co	M = Cu	M = Zn
S1	–29.5	–24.3	–24.2	–28.8
S2	–23.8	–28.7	–29.1	–24.5
S3	–28.8	–28.4	–28.4	–28.9
S4	–28.0	–28.3	–28.5	–28.3
I1	–3.0	–3.0	–2.9	–3.0
I2	1.2	0.9	1.1	1.1
I3	0.9	0.9	1.1	1.1
I4	–2.6	–2.8	–2.7	–2.9
I5	–3.0	–3.1	–2.9	–3.1
I6	1.1	1.4	1.6	1.2
I7	1.2	1.1	1.4	1.2
I8	–2.9	–3.0	–2.9	–3.0

the *a* + *b* axis, which correspond to the stacking axis, were estimated to be 1 order of magnitude larger than those between the molecular stacks. Among the four overlap integrals along the *a* + *b* axis, one (S2 for M = Mn and Zn, S1 for M = Co and Cu) is slightly smaller than the others. Thus, the DMET stack is weakly tetramerized. The energy band structures and Fermi surfaces are shown in Figure 3. The energy band structures consist of four energy bands. Assuming a +0.5 charge per DMET molecule, the first and second lower bands are completely filled and the third and fourth bands come across the Fermi level. Tight-binding energy band calculations suggest that the Fermi surfaces are semimetallic, consisting of electron and hole pockets. It is considered that the semimetallic Fermi

**Figure 3.** Calculated band structure and Fermi surface by tight-binding method.

- (22) (a) Cotton, F. A.; Daniels, L. M.; Huang, P. *Inorg. Chem.* **2001**, *40*, 3576–3578. (b) Matthews, C. J.; Broughton, V.; Bernardinelli, G.; Melich, X.; Brand, G.; Willis, A. C.; Williams, A. F. *New J. Chem.* **2003**, *27*, 354–358.
- (23) (a) Mahmoudkhani, A. H.; Langer, V. *Acta Crystallogr.* **2002**, *E58*, m592–m594. (b) Bremner, C. A.; Harrison, W. T. A. *Acta Crystallogr.* **2003**, *E59*, m425–m426.
- (24) (a) Choi, S.-N.; Lee, Y.-M.; Lee, H.-W.; Kang, S. K.; Kim, Y.-I. *Acta Crystallogr.* **2002**, *E58*, m583–m585. (b) Koman, M.; Siroklin, V.; Ondrejovic, G.; Corradi, A. B.; Battaglia, L. P. *Acta Crystallogr.* **1988**, *C44*, 813–815.
- (25) Fowkes, A.; Harrison, W. T. A. *Acta Crystallogr.* **2004**, *E60*, m59–m61.

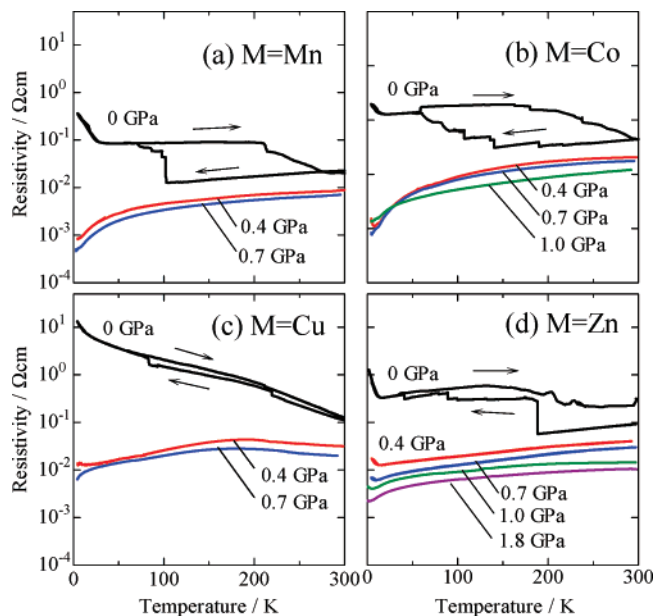


**Figure 4.** Temperature dependence of in-plane resistivities of the M = (a) Mn, (b) Co, (c) Cu, and (d) Zn salts at ambient and applied pressures.

surface is produced by folding the planar Fermi surface of the Q1D stack of DMET molecules due to the tetramerization with four independent molecules in the crystallographic unit cell. This band structure formation resembles that formed by anion ordering at 41 K in (TMTSF)<sub>2</sub>NO<sub>3</sub>.<sup>14</sup>

**Electrical Conduction.** The temperature dependences of the *ab*-plane electrical resistivities of the M = Mn, Co, Cu, and Zn salts are shown in Figure 4a–d at ambient pressure and under pressure applied at room temperature. The arrows in the figures represent the direction of the temperature sweep. At ambient pressure several resistance jumps and hysteresis with respect to the thermal cycle are observed. The temperatures at which the jumps occur differ from sample to sample. The resistivity value at room temperature returns back close to the original value after the thermal cycle. These jumps were suppressed under pressure. These features are quite similar to those found in TMTSF salts,<sup>7</sup> in which the jumps are caused by mechanical kinks induced by thermal contraction during cooling. We consider that the resistivity jumps found here have the same origin as those of TMTSF salts.

Clear signatures of the MI transition, manifesting themselves as abrupt increases of the resistivity, were found at  $T_{MI} = 25$  K for M = Mn,  $T_{MI} = 15$  K for M = Co, and  $T_{MI} = 13$  K for M = Zn. At variant with the resistivity jumps described above, these MI transitions occur at the same temperature for at least five samples of each salt studied. The occurrence of an MI transition is common to DMET salts with tetrahedral ions according to the classification of the electronic behaviors of DMET salts in ref 8. The room-temperature conductivity of the M = Zn salt was slightly higher than that of the other salts. The tendency of  $T_{MI}$  is to change in the order M = Mn > Co > Zn. This tendency corresponds to the ordering of the volumes of unit cells. For M = Mn, Co, and Zn, the interplane resistivity exhibited an MI transition at the same  $T_{MI}$  as the in-plane resistivity; however, the interplane resistivity decreased somewhat more steeply below 100 K than the in-plane resistivity.

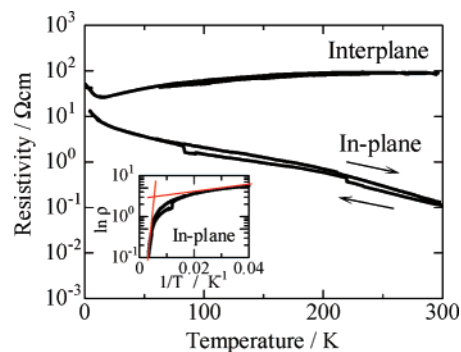


**Figure 5.** Temperature dependence of in-plane and interplane resistivities of the M = Cu salt. (Inset) Arrhenius plot of the temperature dependence of in-plane resistivity.

In contrast, for M = Cu the in-plane resistivity exhibited semiconducting behavior with changing activation energy at ambient pressure. The activation energy changes gradually at about 200 K from 86.0 to 3.8 meV, as shown in the inset of Figure 5. However, the *c*-axis interplane resistivity exhibited metallic behavior, similar to the resistivity of the other salts down to  $T_{MI}$  at ambient pressure, as shown in Figure 5. The interplane resistivity occasionally shows a broad peak at  $\sim 200$  K, above which it is semiconducting, similar to the in-plane case. Hence, the M = Cu salt shows unusual anisotropic conduction; the in-plane conduction is semiconducting while the interplane conduction is metallic from at least  $\sim 200$  K down to the  $T_{MI}$ . There are some examples among layered perovskite cuprates<sup>26</sup> and (TMTSF)<sub>2</sub>PF<sub>6</sub> above 100 K<sup>27</sup> in which the intralayer transport is metallic but the interplane transport is semiconducting. However, the reverse case presented here, being semiconducting in the intralayer transport but metallic in the interplane transport, is the first example to our knowledge. The anisotropy of the resistivity is 200 at room temperature but decreases to as low as 10 at  $T_{MI}$ . The temperature dependence of the resistivity anisotropy has been confirmed using a single-crystal sample by a six-terminal Montgomery-like method.<sup>28</sup> A clear MI transition was observed only for the interplane conduction. The  $T_{MI}$  for M = Cu for the interplane resistivity varies in the range 5–20 K among the measured samples. We ascribe the ambiguity in the  $T_{MI}$  to a mixing of the in-plane contribution into the measured interplane resistivity. Considering the aspect ratio of the sample shape of 0.4 mm in length and 0.1 mm in thickness, such a mixing may occur in the interplane resistivity measurement using the conventional geometry of two electrodes on both sides of the sample surface. Such difficulty in the interplane resistivity measurement becomes critical when the resistivity anisotropy is as low as 10 at low temperatures.<sup>28,29</sup>

Under pressure, the resistivity decreased in all salts, where the resistance jumps were suppressed. The M = Mn, Co, and Zn salts were metallic down to 0.7 K under a pressure of  $\sim 0.4$ ,  $\sim 1.5$ , and  $\sim 2.1$  GPa, respectively. It is intriguing that the pressure needed to suppress the insulating state decreases as

- (26) (a) Ando, Y.; Boebinger, G. S.; Passner, A.; Wang, N. L.; Geibel, C.; Steglich, F. *Phys. Rev. Lett.* **1996**, *77*, 2065–2068. (b) Jiang, C. N.; Baldwin, A. R.; Levin, G. A.; Stein, T.; Almasan, C. C.; Gajewski, D. A.; Han, S. H.; Maple, M. B. *Phys. Rev. B* **1997**, *55*, R3390–R3393.  
 (27) (a) Moser, J.; Gabay, M.; Auban-Senzier, P.; Jerome, D.; Bechgaard, K.; Fabre, J. M. *Eur. Phys. J.* **1998**, *1*, 39–46. (b) Mihaly, G.; Kezmarki, I.; Zamborszky, F.; Forro, L. *Phys. Rev. Lett.* **2000**, *84*, 2670–2673.  
 (28) Ito, H.; Hanada, M.; Tanaka, H.; Kuroda, S.; Mitsumi, M.; Toriumi, K. *J. Phys. Soc. Jpn.* **2005**, *74*, 3334–3339.  
 (29) Montgomery, H. C. *J. Appl. Phys.* **1971**, *42*, 2971–2975.

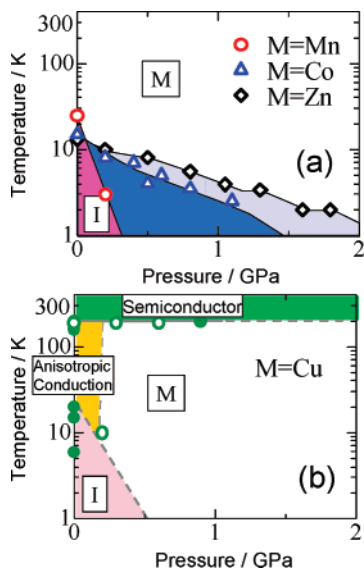


**Figure 6.** (a) Pressure phase diagram of the  $M = \text{Mn}$  (circles),  $\text{Co}$  (triangles), and  $\text{Zn}$  (diamonds) salts. In the phase diagram,  $M$  denotes the metallic phase and  $I$  the insulating phase. (b) Schematic pressure phase diagram of the  $M = \text{Cu}$  salt. Open symbols are based on the in-plane resistivity measurements, and closed symbols are based on the interplane resistivity measurements.

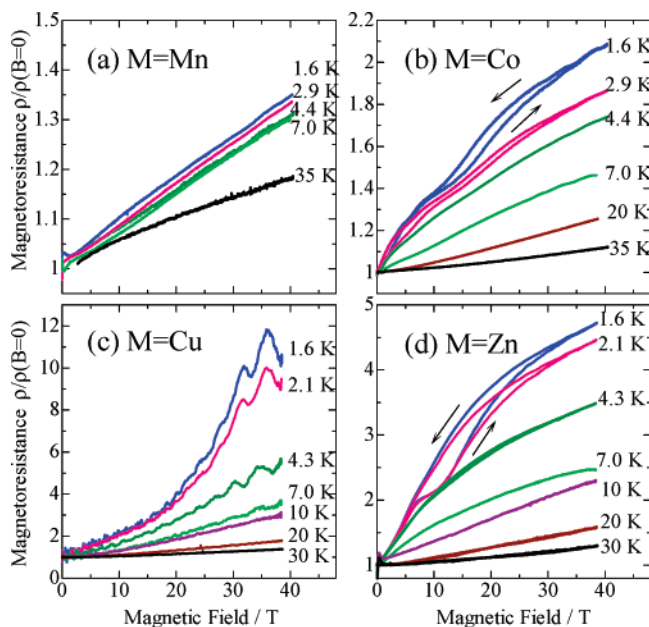


**Figure 7.** Interplane magnetoresistances of the  $M =$  (a)  $\text{Mn}$ , (b)  $\text{Co}$ , (c)  $\text{Cu}$ , and (d)  $\text{Zn}$  salts under a magnetic field perpendicular to the  $ab$  plane.

the MI transition temperature increases. The pressure phase diagram of these three salts is shown in Figure 6a. For  $M = \text{Cu}$  under pressure, the in-plane resistivity was semiconducting around room temperature but became metallic below 200 K, where a semiconductor–metal crossover occurred. The low-temperature insulating phase of the  $M = \text{Cu}$  salt was suppressed under pressures above 0.5 GPa. Under pressure, the anisotropic conduction observed at ambient pressure was suppressed. A schematic pressure phase diagram of the  $M = \text{Cu}$  salt is shown in Figure 6b. For all the salts no indication of superconductivity was found down to 0.7 K, even under applied pressure.

**Magnetoresistance.** Figure 7a, b, c, and d shows the magnetoresistances under pulsed magnetic field for the  $M =$

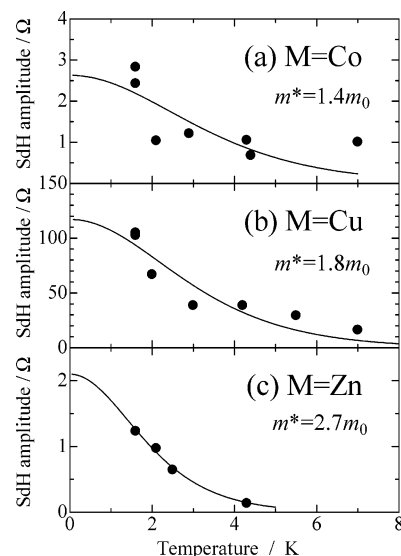


**Figure 8.** Temperature dependence of the magnetoresistance oscillation amplitude of the  $M =$  (a)  $\text{Co}$ , (b)  $\text{Cu}$ , and (c)  $\text{Zn}$  salts at the magnetic field range of 30–35 T. The solid lines are the temperature dependence of the oscillation amplitude after the Lifshitz–Kosevich formula of  $R_T = X/\sinh X$ , where  $X = 14.7(m^*/m_0)(T/B)$ , with the effective mass  $m^*$  shown in the figure ( $m_0$  is the bare electron mass).

**Table 4.** Effective Masses of the Magnetoresistance Oscillations Calculated with the Lifshitz–Kosevich Fits

	oscillation frequency	effective mass (in the unit of the bare electron mass)
$M = \text{Co}$	$240 \pm 10 \text{ T}$	$2.0 \pm 0.8$
$M = \text{Cu}$	$230 \pm 10 \text{ T}$	$1.8 \pm 0.4$
$M = \text{Zn}$	$240 \pm 10 \text{ T}$	$3.0 \pm 1.0$

$\text{Mn}$ ,  $\text{Co}$ ,  $\text{Cu}$ , and  $\text{Zn}$  salts, respectively. Current was applied in the  $c$ -axis interplane direction, and the magnetic field was applied in the same direction. The arrows indicate the direction of the magnetic field sweep. For  $M = \text{Co}$  and  $\text{Zn}$ , large magnetoresistances with hysteresis were observed at low temperatures. The magnetic field width of the hysteresis is larger for  $M = \text{Zn}$ . Above 30 T, the  $M = \text{Co}$  and  $\text{Zn}$  salts exhibited weak oscillatory behaviors with a frequency of  $240 \pm 10 \text{ T}$ . For  $M = \text{Cu}$ , no hysteresis was observed but clear oscillations with a frequency of  $230 \pm 10 \text{ T}$  were observed. The temperature dependence of the amplitude of the magnetoresistance oscillations seems to follow the Lifshitz–Kosevich formula of Shubnikov–de Haas (SdH) oscillation.<sup>30</sup> In Figure 8 we show the temperature dependence of the amplitude fitted with the Lifshitz–Kosevich formula in the magnetic field window of 30–35 T. The effective masses deduced are tabulated in Table 4. Owing to the large error bars in the estimation of the effective mass it is hard to observe a tendency of the effective mass among three salts with and without magnetic ions such as that the salts with magnetic ions have larger effective mass in  $\kappa\text{-(BETS)}_2\text{MCl}_4$  ( $M = \text{Fe, Ga}$ )<sup>31</sup> and  $\beta''\text{-(BEDT-TTF)}_4(\text{H}_3\text{O})\text{M}(\text{C}_2\text{O}_4)_3\text{Y}$  ( $M = \text{Cr, Fe, Ga}$ ;  $\text{Y} = \text{C}_6\text{H}_5\text{NO}_2, \text{C}_6\text{H}_5\text{CN}$ ).<sup>32</sup> On

(30) Shoenberg D. *Magnetic Oscillations in Metals*; Cambridge University Press: Cambridge, 1984.

(31) Uji, S.; Shinagawa, H.; Terai, Y.; Yakabe, T.; Terakura, C.; Terashima, T.; Balicas, L.; Brooks, J. S.; Ojima, E.; Fujiwara, H.; Kobayashi, H.; Kobayashi, A.; Tokumoto, M. *Physica B* **2001**, *298*, 557–561.

(32) Bangura, A. F.; Coldea, A. I.; Singleton, J.; Ardavan, A.; Akutsu-Sato, A.; Akutsu, H.; Turner, S. S.; Day, P.; Yamamoto, T.; Yakushi, K. *Phys. Rev. B* **2005**, *72*, 014543.



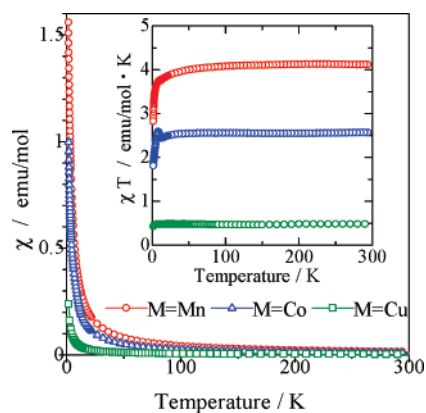


**Figure 9.** Temperature dependence of the dc susceptibility  $\chi$  of the M = Mn (circles), Co (triangles), and Cu (squares) salts. (Inset) temperature dependence of  $\chi T$  for each salt.

the other hand, the M = Mn salt showed a rather weak monotonic magnetoresistance with no hysteresis or oscillatory behaviors.

**dc Magnetic Susceptibility.** The temperature dependences of the magnetic susceptibility  $\chi$  for the M = Mn, Co, and Cu salts are shown in Figure 9 at an applied magnetic field of 10 kOe. The inset shows the temperature dependence of  $\chi T$ . The paramagnetic susceptibilities are well reproduced by the Curie–Weiss model; the Curie constant ( $C$ ) and Weiss temperature ( $\theta$ ) were  $C = 4.13 \text{ emu K mol}^{-1}$  and  $\theta = -1.1 \text{ K}$  for M = Mn,  $C = 2.57 \text{ emu K mol}^{-1}$  and  $\theta = -1.2 \text{ K}$  for M = Co, and  $C = 0.47 \text{ emu K mol}^{-1}$  and  $\theta = -0.6 \text{ K}$  for M = Cu. The Curie constants correspond well with the spins of the divalent metal ions,  $S = 5/2$  for M = Mn,  $S = 3/2$  for M = Co, and  $S = 1/2$  for M = Cu, indicating predominance of contributions to the magnetic susceptibility from d-electron spins over contributions from  $\pi$ -electron spins. The small negative Weiss temperatures of about  $-1 \text{ K}$  indicate antiferromagnetic interactions among magnetic ions. Since the distance between the ions is  $9 \text{ \AA}$ , too far for direct interactions, the interaction may be mediated by  $\pi$  electrons through  $\pi$ -d interactions.  $\chi T$  gradually decreases below  $50 \text{ K}$ , representing the presence of antiferromagnetic interactions among the magnetic spins.

For the M = Zn salt  $\pi$ -electron Pauli susceptibility was observed. The susceptibility was  $\sim 1.0 \times 10^{-3} \text{ emu/mol}$ , 1 order of magnitude larger than that for the metallic DMET salts.<sup>7,33</sup> The dc susceptibility decreased below  $\sim 100 \text{ K}$  and finally vanished near the MI transition, as shown in Figure 10. As the magnetic field for the dc susceptibility measurement is increased, the temperature at which the susceptibility vanishes shifts to higher temperature as shown in the inset of Figure 10. Suppression of the susceptibility at the MI transition implies SDW formation, such as that observed for TMTSF salts.<sup>1,34</sup> Since all salts are isostructural in  $\pi$ -electron electronic structure, the SDW transition should also occur in the other salts. The small upturn of  $\chi T$  at  $\sim 10 \text{ K}$  found for M = Mn, Co, and Cu may be caused the weak contribution of the  $\pi$  electron which turns into the SDW state below  $T_{\text{MI}}$ .

**Electron Spin Resonance.** Figure 11a, b, c, and d shows preliminary measurements of the temperature dependence of

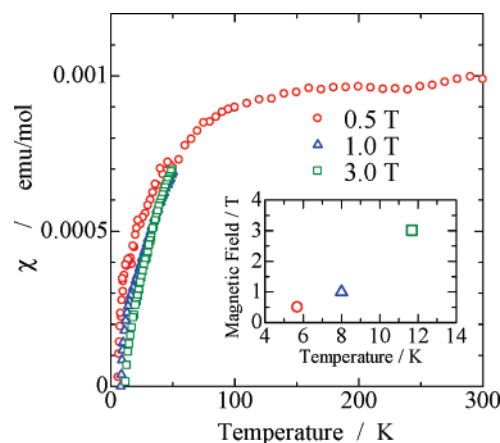


**Figure 10.** Temperature dependence of the dc susceptibility of the M = Zn salt in magnetic fields of 0.5, 1, and 3 T. (Inset) Temperature at which the dc susceptibility vanishes at each magnetic field.

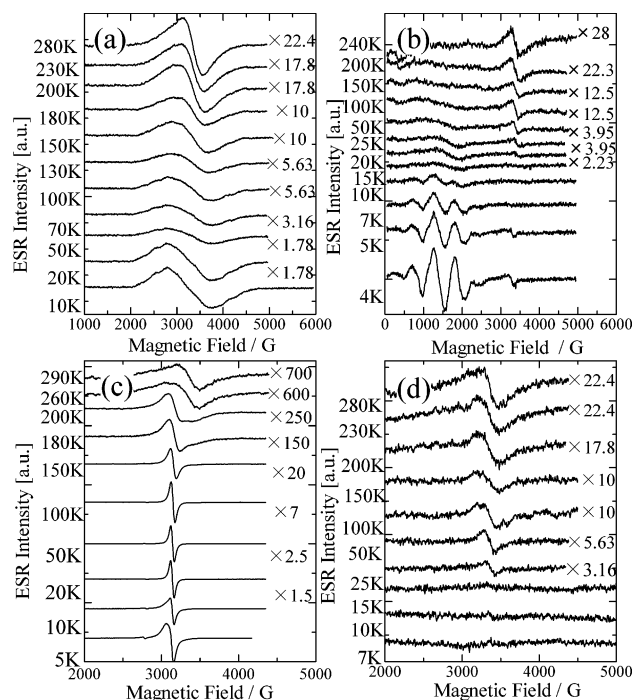


**Figure 11.** Temperature-dependent ESR signals of the M = (a) Mn, (b) Co, (c) Cu, and (d) Zn salts under a magnetic field perpendicular to the  $ab$  plane.

the ESR spectra of the M = Mn, Co, Cu, and Zn salts. The external magnetic field was applied perpendicular to the  $ab$  plane. For M = Mn and Cu a single ESR signal was observed. On the basis of the angular dependence of the  $g$  value and fine structures these signals arise from d electrons. In these salts signals from the  $\pi$  electrons were not observed separately from those of the d electrons, presumably due to either amalgamation of the signals or masking. The ESR spin susceptibility obeys Curie–Weiss behavior with Curie constant ( $C$ ) and Weiss temperature ( $\theta$ ) of  $C = 6.9 \text{ emu K mol}^{-1}$  and  $\theta = -0.11 \text{ K}$  for M = Mn and  $C = 0.69 \text{ emu K mol}^{-1}$  and  $\theta = 0 \text{ K}$  for M = Cu. These parameters are in fair agreement with those determined by dc susceptibility measurements. For M = Cu, the  $g$  value and line width changed at  $\sim 200 \text{ K}$ , where the in-plane resistivity shows a change in activation energy and a semicon-

(33) Kanoda, K.; Takahashi, T.; Kikuchi, K.; Saito, K.; Ikemoto, I.; Kobayashi, K. *Phys. Rev. B* **1989**, *39*, 3996–4003.

(34) (a) Mortensen, K.; Tomkiewicz, Y.; Schultz, T. D.; Engler, E. M. *Phys. Rev. Lett.* **1981**, *46*, 1234–1237. (b) Mortensen, K.; Tomkiewicz, Y.; Bechgaard, K. *Phys. Rev. B* **1982**, *25*, 3319–3325.



ductor–metal crossover occurs under pressure. This may indicate contributions from the  $\pi$ -electron ESR signal above 200 K; a detailed discussion is left for a future study. For both  $M = \text{Mn}$  and  $\text{Cu}$ , narrowing of the line shape was observed with an increase in temperature above the MI transition. The narrowing of the d-electron ESR signal is caused by the  $\pi$ –d interaction, which mediates the exchange interaction between magnetic spins. On the other hand, a  $\pi$ -electron signal at  $g \approx 2$  that vanishes at  $T_{\text{MI}}$  was observed for  $M = \text{Co}$ . ESR signals from  $\text{Co}^{2+}$  were observed at 1000–2000 G with a split line shape. However, integration of the signals failed to reproduce the dc susceptibility of the  $M = \text{Co}$  salt. This may be due to the angle dependence of the ESR signal; further study is now underway. For  $M = \text{Zn}$ , a  $\pi$ -electron signal that vanished at the MI transition was observed. The ESR spin susceptibility is in agreement with the SQUID susceptibility,  $\sim 0.001$  emu/mol. No diverging ESR line width near  $T_{\text{MI}}$  was observed, which is relevant for the SDW transition.<sup>35</sup> This is likely due to the contribution of the Elliot mechanism<sup>33</sup> or an incomplete SDW transition.

## Discussion

The presence of the hysteresis in the magnetoresistance implies the effect of an internal magnetic field on transport properties. Since we find the large magnetoresistance with hysteresis for the  $M = \text{Zn}$  salt with no magnetic ion, the internal magnetic field is not due to the magnetic ion but to the  $\pi$  electron. The MI transitions of these salts are considered to be caused by an SDW transition owing to the nesting of Fermi surfaces. Considering the Q1D electronic structure calculated for the salts, it is likely that the nesting of the Q1D Fermi surfaces occurs like those found in TMTSF and DMET salts.<sup>7,8</sup> The large magnetoresistance with hysteresis is reminiscent of the field-induced SDW transition.<sup>7,9,11</sup> In terms of the field-induced SDW transition, imperfect nesting creates small pockets in which Landau levels are formed under magnetic fields, which give rise to first-order transitions between field-induced sub-phases, causing hysteretic behavior with respect to the magnetic field sweep. The disappearance of the paramagnetic ESR signal of the  $\pi$  electrons below the MI transition for the  $M = \text{Zn}$  and  $\text{Co}$  salts supports the conclusion that the SDW transition is the origin of the MI transition. The decrease in the dc susceptibility below 100 K for the  $M = \text{Zn}$  salt implies the effect of antiferromagnetic fluctuations existing at high temperatures above  $T_{\text{MI}}$ . As the magnetic field is increased, the temperature at which the dc susceptibility vanishes shifts to higher temperatures as shown in the inset of Figure 10, probably because the SDW transition is completed with the help of the magnetic field. The resistivity below  $T_{\text{MI}}$  increases exponentially with activation energies of  $4 \pm 1$ ,  $0.5 \pm 0.2$ , and  $1.0 \pm 0.5$  meV for  $M = \text{Mn}$ ,  $\text{Co}$ , and  $\text{Zn}$ , respectively. The value for the  $M = \text{Mn}$  salt is close to the mean-field BCS value of the SDW gap of  $1.76 k_{\text{B}}T_{\text{MI}}$  opening in the electronic spectrum, but those for  $M = \text{Co}$  and  $\text{Zn}$  are smaller than the mean-field BCS values. The origin of the difference in the activation energy among  $M = \text{Mn}$  salt and  $M = \text{Co}$  and  $\text{Zn}$  salts needs further study. This is

probably related to the imperfect nature of the SDW transition, as discussed for  $(\text{TMTSF})_2\text{NO}_3$ .<sup>7,36</sup>

Tight-binding band calculations determined the size of the electron and hole pockets to be 2.5% of the first Brillouin zone, which corresponds to an SdH oscillation frequency of 110 T. The observed frequencies of the magnetoresistance oscillation are twice as large as this value. The discrepancy in the frequency may be caused by the Fermi surface reconstruction at the SDW transition like  $\beta''$ -(BEDT-TTF)<sub>2</sub>AuBr<sub>2</sub>.<sup>37</sup> Another interpretation is that considering the Q1D Fermi surfaces the oscillations above 30 T may be understood in terms of the so-called rapid oscillations often observed for TMTSF salts.<sup>38</sup> If a magnetic breakdown of the semimetallic Fermi surfaces occurs, the Q1D planar Fermi surfaces are retrieved in high fields, giving rapid oscillations at a similar frequency to those of Q1D TMTSF salts, as in the case of  $(\text{TMTSF})_2\text{NO}_3$ .<sup>39</sup> However, at variance with the TMTSF salts, in which the maximum of the oscillation amplitude appears at 3 K<sup>38</sup>, the oscillation amplitude in the salts seems to obey the temperature dependence of the Lifshits–Kosevich formula as shown in Figure 8. A recent report shows that under pressure the oscillation amplitude also obeys the Lifshits–Kosevich formula in  $(\text{TMTSF})_2\text{NO}_3$ .<sup>40</sup>

The magnetoresistance of the  $M = \text{Mn}$  salt was small in comparison with the other salts, and SdH oscillation was absent. The larger spin of Mn may affect the SDW ordering at low temperature, which suppresses the magnetoresistance and oscillations. Suppression of the MI transition at relatively low pressure in the  $M = \text{Mn}$  salt may also be caused by the Mn spins.

The anisotropic conduction in the  $M = \text{Cu}$  salt, in which conduction in the in-plane direction is semiconducting while that in the interplane direction is metallic for temperatures down to  $T_{\text{MI}}$ , is intriguing, and its origin will require further investigation. This phenomenon may indicate an interaction between conduction electrons and  $\text{Cu}^{2+}$  spins. Another explanation may be that it is due to a contribution from weak localization in the in-plane conduction that does not affect the interplane conduction. The temperature dependence of the in-plane resistivity can be scaled with the logarithmic dependence of the weak localization below 100 K. As noted in the crystal structure section, Jahn–Teller distortion is present in the  $\text{CuCl}_4^{2-}$  anion. This may introduce disorder or a weak superstructure in the  $ab$  plane, which causes localization of the electronic state by giving rise to additional scattering. The Jahn–Teller distortion of the  $\text{CuCl}_4^{2-}$  anion may be dependent on temperature and also

(35) Tomic, S.; Jerome, D.; Cooper, J. R.; Bechgaard, K. *Synth. Met.* **1988**, *27*, B645–B649.

(36) (a) Tomic S.; Cooper J. R.; Kang W.; Jerome D.; Maki K. *J. Phys. I* **1991**, *1*, 1603–1625. (b) Basletic, M.; Biskup, N.; Korin-Hamzic, B.; Tomic, S.; Hamzic, A.; Bechgaard, K.; Fabre, J.-M. *Europhys. Lett.* **1993**, *22*, 279–285.

(37) (a) Doport, M.; Singleton, J.; Pratt, F. L.; Caulfield, J.; Hayes, W.; Perenboom, J. A. A. J.; Deckers, I.; Pitsi, G.; Kurmoo, M.; Day, P. *Phys. Rev. B* **1994**, *49*, 3934–3943. (b) House, A. A.; Harrison, N.; Blundell, S. J.; Deckers, I.; Singleton, J.; Herlach, F.; Hayes, W.; Perenboom, J. A. A. J.; Kurmoo, M.; Day, P. *Phys. Rev. B* **1996**, *53*, 9127–9136.

(38) (a) Brooks, J. S.; O'Brien, J.; Starrett, R. P.; Clark, R. G.; McKenzie, R. H.; Han, S.-Y.; Qualls, J. S.; Takasaki, S.; Yamada, J.; Anzai, H.; Mielke, C. H.; Montgomery, L. K. *Phys. Rev. B* **1999**, *59*, 2604–2608. (b) Vignolles, D.; Ulmet, J. P.; Audouard, A.; Naughton, M. J.; Fabre, J.-M. *Phys. Rev. B* **1999**, *61*, 8913–8916.

(39) (a) Audouard, A.; Goze, F.; Dubois, S.; Ulmet, J. P.; Brossard, L.; Askenazy, S.; Tomic, S.; Fabre, J.-M. *Europhys. Lett.* **1994**, *25*, 363–368. (b) Kang, W.; Behnia, K.; Jerome, D.; Balicas, L.; Canadell, E.; Ribault, M.; Fabre, J. M. *Europhys. Lett.* **1995**, *29*, 635–640. (c) Kishigi, K.; Machida, K. *Phys. Rev. B* **1997**, *53*, 5461–5464.

(40) Vignolles, D.; Audouard, A.; Nardone, M.; Brossard, L.; Bouguessa, S.; Fabre, J.-M. *Phys. Rev. B* **2005**, *71*, 020404(R)–1–4.

change under pressure,<sup>41</sup> which may explain the unusual transition at 200 K and suppression of the anisotropic conduction under pressure in terms of the structural phase transition. To clarify the origin of the peculiar behavior of the  $M = \text{Cu}$  salt, X-ray and Raman studies are in progress.

### Summary

We synthesized a new series of DMET salts with metal halide ions and TCE. An MI transition was observed, caused by imperfect nesting of semimetallic Fermi surfaces. A tentative pressure phase diagram was postulated from resistivity measurements under pressure. For the nonmagnetic  $M = \text{Zn}$  salt, we observed a large magnetoresistance with hysteresis, implying FISDW behavior. For the  $M = \text{Co}$  salt, the transport behavior was similar to that for  $M = \text{Zn}$ , indicating that the interaction between the  $\pi$  and d electrons is not significant for the  $M = \text{Co}$  salt. The transport properties of the  $M = \text{Mn}$  and  $\text{Cu}$  salts were different from those of the  $M = \text{Zn}$  and  $\text{Co}$  salts. The  $M = \text{Mn}$  salt shows suppressed monotonic magnetoresistance. The  $M = \text{Cu}$  salt shows clear SdH oscillations but no hysteresis in

magnetoresistance. It is remarkable that the  $M = \text{Cu}$  salt shows peculiar anisotropic conduction at ambient pressure with interplane metallic conduction and in-plane semiconducting conduction with an unusual phase crossover at 200 K. These behaviors can be understood in terms of  $\pi$ -d interactions; however, involvement of the Jahn-Teller distortion of  $\text{CuCl}_4^{2-}$  can also be considered.

**Acknowledgment.** The authors thank Profs. H. Tajima, T. Mori, and Y. Suzumura for valuable discussions on the electronic band structure and origin of the MI transition. We thank Dr. M. Watanabe for discussion on the crystal structure. This research was supported by the Scientific Research on Priority Areas 'Novel Functions of Molecular Conductors Under Extreme Conditions', 16038215 and 18028012, of Education, Culture, Sports, Science, and Technology of Japan.

**Supporting Information Available:** Crystallographic information files (CIF) for  $(\text{DMET})_4\text{M}^{\text{II}}\text{Cl}_4(\text{TCE})_2$  ( $M = \text{Mn}, \text{Co}, \text{Cu}, \text{Zn}$ ). This material is available free of charge via the Internet at <http://pubs.acs.org>.

(41) (a) Moritomo, Y.; Tokura, Y. *J. Chem. Phys.* **1994**, *101*, 1763–1766. (b) Nishijima, Y.; Mashiyama, H. *J. Phys. Soc. Jpn.* **2000**, *69*, 3581–3588.

JA070672Q